Failures at Attachment Holes in Brittle Matrix Laminates

GUY M. GENIN AND JOHN W. HUTCHINSON*
Division of Engineering and Applied Science
Harvard University
29 Oxford Street
Cambridge, MA 02138

(Received October 24,1997)
(Revised July 19, 1998)

ABSTRACT: Mechanical attachments for a brittle-matrix fiber-reinforced cross-ply composite are analyzed. Two model problems are considered: first, a bolt-loaded strut, and second, an infinitely-wide plate with evenly-spaced bolts. The possible failure mechanisms for the strut are identified, and the influence of bolt size, bolt location, bolt elasticity, and interfacial friction on these failure mechanisms and the associated failure loads are evaluated. The bolt spacing for the plate is identified that best takes advantage of a SiC/MAS cross-ply's ability to redistribute stresses through the mechanism of matrix cracking.

Boundary value problems are solved using the finite element method. The cross-ply's constitutive behavior is described by the model of Genin and Hutchinson [1].

KEY WORDS: "ductile" ceramic matrix composites, mechanical attachments, bolt-loaded hole, failure mechanisms, failure loads, stress redistribution due to matrix cracking.

1. INTRODUCTION

A FUNDAMENTAL DIFFICULTY faced when incorporating ceramic matrix composite (CMC) components into design is the attachment of the CMC components to each other and to components made of other materials. Drilling a hole through a CMC laminate and applying force to the laminate through a bolt leads to stress concentrations that accelerate matrix cracking. Since matrix cracking can affect failure by either relieving or intensifying stresses near stress-concentrating features [1], design with ceramic matrix composites must be based on analysis that accounts for the stress redistribution caused by matrix cracking.

*Author to whom correspondence should be addressed.

0021-9983/99/17 1600–20 $10.00/0

The focus of this study is development of an understanding of how CMCs perform in the vicinity of bolts, with an emphasis on the influence of matrix cracking on this performance. Two model problems are considered: a bolted CMC strut serves as a model for identifying the influence of geometric and material parameters on failure mechanisms in the vicinity of fasteners, and an infinitely wide, uniformly loaded plate fastened with evenly spaced bolts is studied to determine how these competing mechanisms influence optimal design.

The laminate strut is loaded axially through bolts inserted into holes near the ends of the strut, as shown in Figure 1(a). The infinite laminate plate, shown in Figure 2(a), is loaded similarly. Three sets of parameters are relevant to the problems: (1) the specimen dimensions h/r and w/r (s/r for the plate); (2) the material properties of the bolt and the laminate; and (3) friction at the interface between the bolt and the laminate. In both problems, the laminate's constitutive behavior is modeled using the model of Genin and Hutchinson [1], which will be discussed in Section 2. The bolts are assumed either to be rigid, or to remain linear-elastic at all loads.

Previous work on the model strut that addresses some of the above factors is reviewed in the following two sections. Section 1.1 reviews the results of analytical and numerical investigations of how the aforementioned parameters influence the

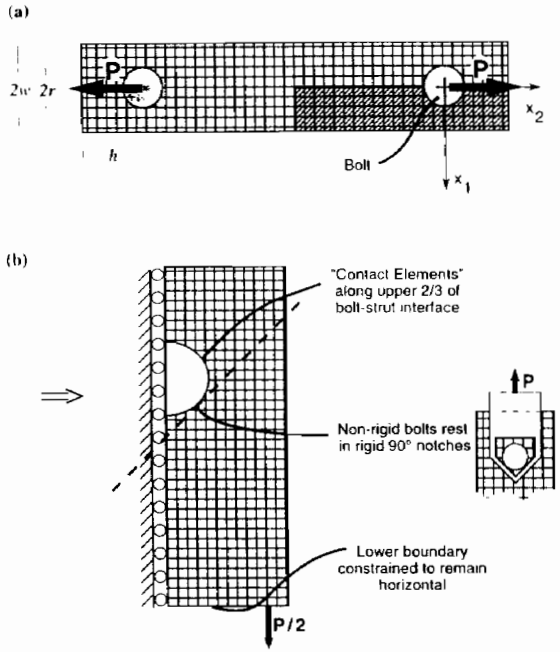

Figure 1. *(a) A CMC strut and (b) the model used in the analyses.*

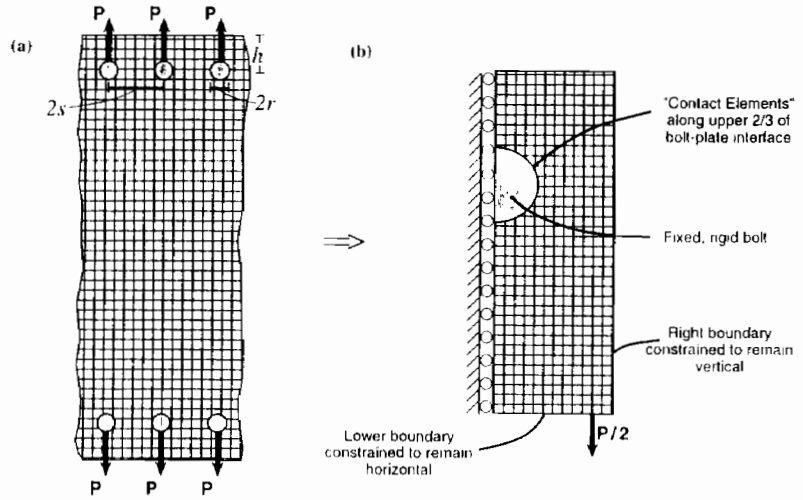

Figure 2. *(a) A CMC plate and (b) the model used in the analyses.*

stress distribution at the bolt-strut interface of a linear elastic strut, and also describes some attempts to model the "ductility" of the strut due to matrix cracking. Section 1.2 reviews the failure mechanisms observed in components of this type.

1.1 Previous Analytical Work on Bolted Joints in CMCs

The fastener illustrated in Figure 1 has been studied extensively [2–14]. Analyses typically employ plane stress to model the laminate's behavior. The vast majority of work on fasteners is based on linear elastic analyses, and has focused on determining the stress field along the boundary between the bolt and the strut. In finite element analyses, the radial stress distribution along the boundary between an isotropic strut and a rigid, frictionless bolt is commonly modeled with a cosine distribution over a 180° region of contact [e.g., 2–4] after Bickley [5]. The actual distribution of normal stresses is fairly close to this for mildly orthotropic struts loaded with rigid bolts when the interface between the bolt and the strut is frictionless [3,6–10]. The tangential stresses in the strut at the hole boundary are compressive beneath the bolt [the point $(0,-r)$ in Figure 1(a) for a strut loaded in tension], and tensile above the bolt. The peak tensile stresses typically occur near the point $(r,0)$. Several authors have noted that friction relieves stresses above the bolt [at $(0,r)$] and intensifies the maximum stress concentration [3,8,9]. Hyer et al. [3] concluded from an analysis neglecting interfacial friction that the elastic properties of the bolt only mildly affect the stress distribution in the strut; the maximum tangential stress along the hole boundary decreases slightly as the elastic modulus of the bolt decreases.

Two efforts to model material nonlinearity in the cross-ply from which the strut in Figure 1 is constructed have used a phenomenological approach, and have qualitatively reproduced experimental observations. Both Serabian and Oplinger [10], and Chang et al. [11], used the linear elastic behavior of a cross-ply in tension and a curve fit of the cross-ply's behavior in shear in their constitutive relations. Serabian and Oplinger's analysis produced a strain field qualitatively similar to that which they observed experimentally. Chang et al. found that the stresses from their analysis, when entered into a failure criterion, predicted the failure loads they observed more accurately than did the stresses from their linear elastic analysis, reported in Reference [4].

1.2 Identification of Failure Mechanisms

CMC struts like that of Figure 1 can fail in three modes, as depicted in Figures 3 (a–c) [e.g., 12,13]. A fourth possible mode of failure, depicted in Figure 3(d), has never been observed in CMCs, but has been observed in a polymer matrix composite [14].

Cady et al. [12], mapped the range of specimen sizes over which each of the first three mechanisms in Figure 3 is most likely to occur through experiments on struts of a SiC/CAS cross-ply. The shear mode of failure shown in Figure 3(a) occurs in struts with a large width w compared to the distance h from the center of the bolt to the top edge of the strut. The normal mode of failure in Figure 3(b) occurs for narrow struts in which the ratio h/w is large. Bearing failure as shown in Figure 3(c) occurs when h and w are both large compared to the diameter of the bolt.

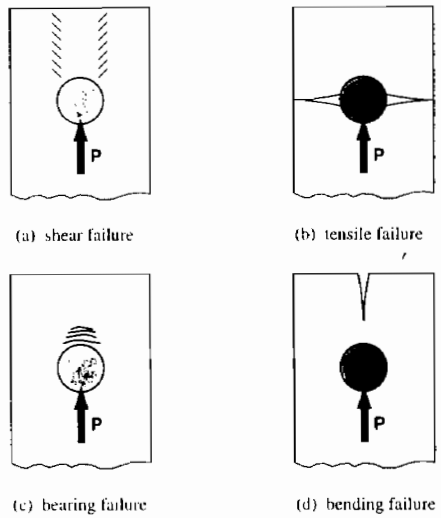

Figure 3. *Failure mechanisms for fastened struts.*

The "bending" failure shown in Figure 3(d) was observed by Matthews et al., in a fiber-reinforced polymer matrix cross-ply composite comprised of woven graphite fibers in an epoxy matrix [14]. This mode of failure occurred only in specimens which first failed with a bearing failure like that of Figure 3(c).

1.3 Overview

The material model used to describe the behavior of the CMC is discussed in Section 2. The strut depicted in Figure 1 will be analyzed in Section 3. The effect of relative strut dimensions, bolt elasticity, and interfacial friction on failure mechanisms and failure loads for a CMC strut is determined. Design optimization based on the nonlinear behavior exhibited by CMCs is performed in Section 4 for the plate shown in Figure 2, where the optimum spacing for bolts supporting a CMC plate will be ascertained. The influence of material nonlinearity on optimal design is highlighted.

2. MATERIAL MODEL

This section discusses the material model used to describe the behavior of the CMC. Section 2.1 reviews the plane stress constitutive framework for symmetrically stacked brittle-matrix laminates developed in Reference [1]. This framework will be specialized to the case of a laminate stacked with a [0/90] configuration, and fit to uniaxial stress-strain data gathered for a SiC/MAS laminate by McNulty and Zok [15,16]. The failure criterion which will be used is discussed in Section 2.2.

2.1 Constitutive Model

The constitutive model of Genin and Hutchinson [1], specialized to the case of a cross-ply laminate, is considered. For a cross-ply, the constitutive model is based on the three uniaxial curves shown in Figure 4. The stress-strain curve from a tensile test performed parallel to the fibers in a cross-ply laminate is denoted by $\varepsilon_I = f_0(\sigma_I)$, and the transverse strain from this same test is written as $\varepsilon_{II} = f_{0T}(\sigma_I)$. Similarly, the strain in the loading direction for a uniaxial tension test conducted at 45° to the fiber directions is expressed as $\varepsilon_I = f_{45}(\sigma_I)$, and the function describing strain transverse to the loading direction in this test is denoted $f_{45T}(\sigma_I)$.

The model begins with the following proposal for proportional multiaxial loading when the principal axes of stress and strain are aligned with the fibers in the cross-ply:

$$\begin{aligned} \varepsilon_I &= f_0(\sigma_I) + f_{0T}(\sigma_{II}) \\ \varepsilon_{II} &= f_0(\sigma_{II}) + f_{0T}(\sigma_I) \end{aligned} \tag{1}$$

For loading in which the principal axes of stress are aligned in the symmetry

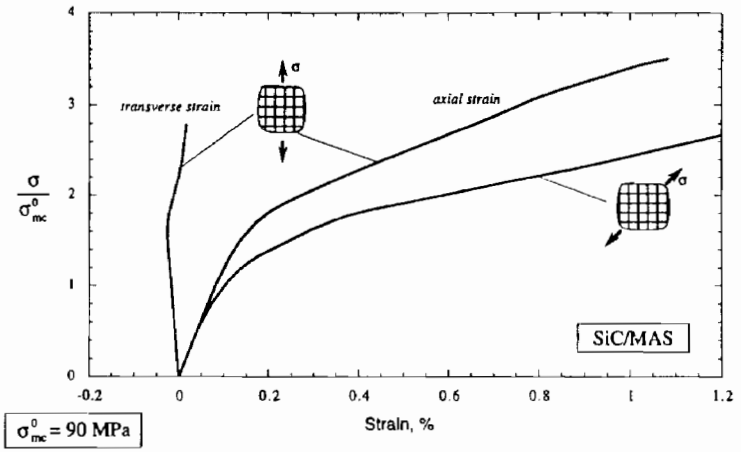

Figure 4. *Uniaxial stress-strain curves for a cross-ply ceramic matrix composite (SiC/MAS). Data are from McNulty and Zok [15,16].*

axes 45° from the fibers in a cross-ply, the strains share the same principal axes, and are given by:

$$\begin{aligned} \varepsilon_I &= f_{45}(\sigma_I) + f_{45T}(\sigma_{II}) \\ \varepsilon_{II} &= f_{45}(\sigma_{II}) + f_{45T}(\sigma_I) \end{aligned} \tag{2}$$

By considering the case of equibiaxial loading, in which $\sigma_I = \sigma_{II} \equiv \sigma$, and equating the first strain invariant [proportional to $(\varepsilon_I + \varepsilon_{II})$] calculated in the two sets of symmetry axes, a condition is derived which reveals that only three of the four stress-strain curves for a CMC cross-ply are independent:

$$f_{45T}(\sigma) = f_0(\sigma) + f_{0T}(\sigma) - f_{45}(\sigma) \tag{3}$$

The constitutive model used follows Equations (1) and (2) exactly for principal loads applied in the axes of symmetry, and interpolates between these axes for all other loadings. The interpolation is based on the stresses. To facilitate this, begin by defining $\Sigma_0(\varepsilon_I, \varepsilon_{II})$ as the inverse of Equations (1), such that

$$\begin{aligned} \sigma_I &= \Sigma_0(\varepsilon_I, \varepsilon_{II}) \\ \sigma_{II} &= \Sigma_0(\varepsilon_{II}, \varepsilon_I) \end{aligned} \tag{4}$$

The reduction in stresses due to matrix cracking at prescribed ε_I and ε_{II}, when the principal loading axes coincide with the fiber directions, is the difference between the stresses that would result if no cracking occurred and the actual stress state (σ_I, σ_{II}). The "stress deficits" for loading in the fiber axes are defined as:

$$\Delta\sigma_I^0 = \frac{E_0}{(1-\nu_0^2)}(\varepsilon_I + \nu_0\varepsilon_{II}) - \Sigma_0(\varepsilon_I, \varepsilon_{II})$$
$$\Delta\sigma_{II}^0 = \frac{E_0}{(1-\nu_0^2)}(\varepsilon_{II} + \nu_0\varepsilon_I) - \Sigma_0(\varepsilon_{II}, \varepsilon_I) \quad (5)$$

where E_0 and ν_0 are the elastic modulus and Poisson's ratio for uniaxial loading parallel to the fibers.

When the principal axes of loading lie at 45° to the fiber directions, the stress deficits in these axes are given by:

$$\Delta\sigma_I^{45} = \frac{E_{45}}{(1-\nu_{45}^2)}(\varepsilon_I + \nu_{45}\varepsilon_{II}) - \Sigma_{45}(\varepsilon_I, \varepsilon_{II})$$
$$\Delta\sigma_{II}^{45} = \frac{E_{45}}{(1-\nu_{45}^2)}(\varepsilon_{II} + \nu_{45}\varepsilon_I) - \Sigma_{45}(\varepsilon_{II}, \varepsilon_I) \quad (6)$$

Here, E_{45} is the elastic modulus for uniaxial loading in the axes at 45° to the fiber directions, $\nu_{45} = 1 - (1 - \nu_0)(E_{45}/E_0)$, and the combined equations $\sigma_I = \Sigma_{45}(\varepsilon_I,\varepsilon_{II})$ and $\sigma_{II} = \Sigma_{45}(\varepsilon_{II},\varepsilon_I)$ form the inverse of Equation (2).

For principal strains $(\varepsilon_I,\varepsilon_{II})$ in principal axes oriented at an arbitrary angle θ from the fiber directions, the principal axes of the stress deficits are taken to coincide with the principal strain axes. The stress deficits in these axes are assumed to be given by interpolation between the stress deficits in the 0° and 45° orientations according to:

$$\Delta\sigma_I = \Delta\sigma_I^0 \cos^2 2\theta + \Delta\sigma_I^{45} \sin^2 2\theta$$
$$\Delta\sigma_{II} = \Delta\sigma_{II}^0 \cos^2 2\theta + \Delta\sigma_{II}^{45} \sin^2 2\theta \quad (7)$$

Upon rotating back to the fiber axes, one obtains the plane stress relation for stresses associated with proportional straining to $(\varepsilon_1,\varepsilon_2,\gamma_{12} = 2\varepsilon_{12})$:

$$\sigma_1 = \frac{E_0}{(1-\nu_0^2)}(\varepsilon_1 + \nu_0\varepsilon_2) - \Delta\sigma_I \cos^2\theta - \Delta\sigma_{II} \sin^2\theta$$
$$\sigma_2 = \frac{E_0}{(1-\nu_0^2)}(\varepsilon_2 + \nu_0\varepsilon_1) - \Delta\sigma_I \sin^2\theta - \Delta\sigma_{II} \cos^2\theta \quad (8)$$
$$\tau = \frac{E_{45}}{2(1+\nu_{45})}\gamma_{12} - (\Delta\sigma_I - \Delta\sigma_{II}) \sin\theta\cos\theta$$

2.1.1 MODEL CMC

The material studied in this paper is a cross-ply laminate that exhibits an apparent "ductility" when loaded in uniaxial tension, as shown in Figure 4. The laminae are constructed of aligned SiC fibers embedded in a glass (MAS) matrix, and the laminate is constructed of a series of these laminae arranged such that the fiber directions of neighboring layers are perpendicular to one another. The curves in Figure 4 for loading parallel to one set of fibers are from McNulty and Zok [15]; the curve for loading at 45° to the fiber directions is derived from the results of a Iosipescu shear test performed by McNulty and Zok [16] using a formulation that is presented in Reference [17]. In this paper, all stresses are normalized by the proportional limit for loading parallel to one set of fibers in the cross-ply, $\sigma_{mc}^0 = 90$ MPa.

The nonlinear material behavior is modeled in the analyses that follow by fitting the constitutive model described above to the stress-strain curves in Figure 4. Linear elasticity is used for all compressive stresses. The stress-strain curves are extrapolated linearly for stresses and strains that exceed the limits of the data in tension.

2.2 Failure Criterion

The criterion adopted in this paper is that the laminate will fail when the normal strain in the direction of one set of fibers at some point equals the uniaxial failure strain observed in a tensile specimen. This is equivalent to a maximum normal stress criterion for the fibers in the material. Since this failure criterion is very poor for prediction of compressive failure in fiber-reinforced cross-plies [18], the development of the bearing failure mechanism of Figure 3(c) (which requires a compressive failure above the bolt) is not monitored. Instead, this work focuses on the remaining three mechanisms.

The justification for the maximum strain criterion is as follows: when a brittle matrix laminate is saturated with matrix cracks, the fibers carry the entire applied load, and are largely debonded from the matrix material. The strain in the fibers once the matrix is saturated with cracks is thus the difference between the macroscopic strain as predicted by the continuum constitutive model and the initial residual strain in the fibers from the manufacturing process for the laminate. If the fibers remain linear-elastic until the failure load, then a maximum strain failure criterion for the fibers is equivalent to a maximum normal stress criterion. Therefore, assuming the matrix material saturates with cracks before the laminate fails, the level of strain necessary to raise the fibers from their initially compressive stress state to their in situ failure stress is the failure strain for a uniaxial specimen of the material. The uniaxial failure strain from a tensile specimen is thus used in this study as the critical failure strain.

The failure criterion is based on the premise that a laminate fails when the first fibers in the laminate break in tension. This assumption oversimplifies actual conditions in a cross-ply [e.g., 19,20].

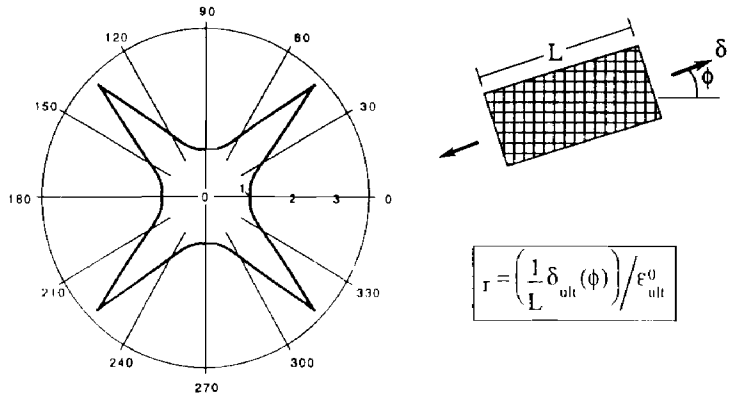

Figure 5. *Axial failure strain for SiC/MAS stretched at an angle ϕ from one set of fibers, as predicted by a maximum normal strain criterion.*

Predictions of the displacements necessary to stretch plates of the SiC/MAS cross-ply to failure are plotted in Figure 5 as a function of the angle ϕ between the loading direction and the orientation of one set of the cross-ply's fibers. The failure criterion predicts a failure strain for loading at 45° to the fiber directions that is about three times the strain needed to fail the fibers in uniaxial loading parallel to one set of fiber axes. This is an overprediction: for loadings applied at ±45° to the fiber axes, CMCs like the SiC/MAS composite studied in this paper typically fail at strains on the order of 0.9–1.5 times the failure strain for loading parallel to one set of fibers [e.g., 21,22]. The discrepancy here indicates that a mechanism other than fiber failure is dominant for loading at 45° to the fiber directions. Accordingly, the shear strength of the cross-ply and thus the resistance to the "shear" mode of failure is overpredicted in the analyses in this paper.

3. PREDICTION OF FAILURE MECHANISMS IN CMC STRUTS

The failure criterion described in Section 2.2 is applied to the results of finite element analyses of the bolted strut of Figure 1. The failure loads and failure mechanisms predicted by these analyses are compared for struts of varying geometries, and the effects of elasticity in the bolt and friction at the interface between the bolt and the strut are investigated.

3.1 Numerical Model

The influence of strut geometry, bolt elasticity, and interfacial friction on failure modes and failure loads is assessed through finite element analyses. The mathematical model chosen for the analyses exploits the symmetry of the strut about

both its horizontal and vertical mid-planes, as depicted in Figure 1(b). Along the bottom of the model in Figure 1(b), the vertical (x_2-direction) displacements are constrained to be the same, and the shear traction vanishes. The lower boundary carries a net vertical force of P/2. The left-hand boundary of the model in Figure 1(b) is free of shear-traction, and is constrained from moving in the x_1-direction.

For analyses in which the bolt is not assumed rigid, the boundary conditions on the bolt approximate a loading apparatus used in the experiments of Cady et al. [12], in which the bolt rests in a 90° notch in a rigid loading fixture, as pictured in Figure 1(b). To model this fixture, nodes on the finite element mesh for the bolt that lie close to the contact point between the bolt and the loading apparatus are constrained to move along the 45° line shown in Figure 1(b). The bolt is assumed to fit perfectly into the hole in the unloaded state.

Because of the interface between the bolt and the plate, the finite element mesh and its boundary conditions at each loading increment must be found as part of the solution; iteration is required even for loads in the linear range. The numerical procedure begins with a guess as to which nodes on the plate will be "in contact" with corresponding nodes on the bolt after a load is applied.

Stresses and displacements are calculated for this initial mesh, and are checked to ensure that none of the elements assumed to be in contact are predicted to carry tension normal to the contact plane. Nodes in regions assumed to be free of contact are checked to verify that no interpenetration occurs. Interpenetration occurs if the displacement component of a node on the bolt boundary in the direction of the initial outward normal to the bolt boundary exceeds that of the corresponding node on the strut boundary in this direction. If the check reveals that a portion of the bolt-strut boundary is in tension, the analysis is repeated with that portion of the boundary assumed to be traction-free; if the check reveals that nodes from the bolt and the plate interpenetrate, the analysis is repeated with those nodes assumed to be in contact. Once the closest approximation to the proper mesh is determined, the analysis continues with the next loading increment.

3.2 Influence of Strut Geometry on Failure Load and Failure Mechanism

Finite element analyses are run to gain insight into the material response for a range of strut geometries. In these analyses, the bolt is assumed to be rigid, and the interface between the bolt and the strut is assumed to be frictionless.

3.2.1 BOLT DEPTH, h/r

To establish the effect of varying the distance h from the center of the bolt to the top of the strut, two analyses are run with the above procedure for SiC/MAS struts of identical widths $w/r = 4$, but different bolt depths h/r. Contours of the maximum principal stresses and of the intensity of matrix cracking for the loads at which each of the two struts are predicted to fail are shown in Figure 6. The measure of the in-

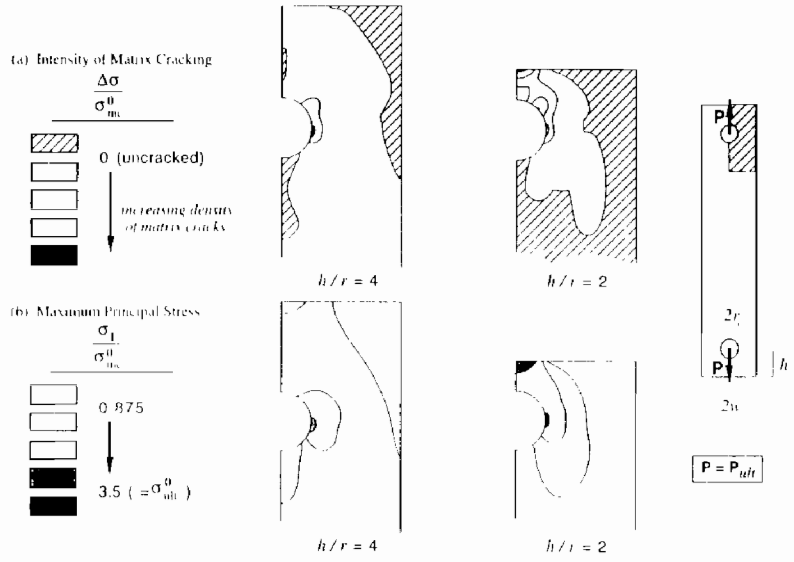

Figure 6. *Effect of bolt depth* h *on (a) matrix cracking and (b) stress distribution at failure load,* P_{ult}; w/r = 4.

tensity of matrix cracking $\Delta\sigma$ used in Figure 6(a) is the square root of the sum of the squares of the "principal stress deficits" defined in Equation (7):

$$\Delta\sigma \equiv \sqrt{(\Delta\sigma_I)^2 + (\Delta\sigma_{II})^2} \tag{9}$$

The contours shown in Figure 6 reveal how the two struts carry axial loads, and the differences in their responses to this loading. Studying first the stress distribution at the point of failure in the strut with largest bolt depth h ($h/r = 4$), which is shown in the lower-left corner of Figure 6, the observation is made that the two regions in the strut carrying the most load are (1) the material at the hole boundary by the thinnest section of the strut, and (2) the material at the top center of the strut. The plot of matrix crack intensity for this strut, which is shown in the upper-left corner of Figure 6, reveals that matrix cracking is most intense at the point of maximum stress on the hole boundary. Slight cracking in shear is evident in this plot, emanating near the 45° point on the hole boundary and spreading very slightly upwards above the bolt. When the failure criterion is met, the entire width of the strut is predicted to have undergone matrix cracking at points lower than a few bolt radii beneath the hole. The location at which the failure criterion is first met is on the hole boundary, where the tensile stresses are highest, and the strut will clearly fail by a "tensile"-type failure originating from this point.

Halving the bolt depth h significantly alters the way the strut carries axial load. The stress distribution for the strut with $h/r = 2$, shown in the lower-right corner of Figure 6, reveals a large increase in the stress concentration at the top of this strut relative to that in the longer strut; the point of maximum tensile stress here is in fact the center of the strut's upper edge. If the material between the top of the bolt and the upper edge of the strut is thought of as a beam, the reason for this increase in the stress concentration becomes clear: moving the bolt closer to the top of the strut reduces the bending stiffness of the "beam" of material above the hole, and as a consequence increases the tensile stress at the beam's outermost point. The failure criterion is met at this outermost point, and this strut fails by the "bending" mode of failure.

The plot of matrix cracking intensity reveals that, in addition to increasing the intensity of matrix cracking at the top of the strut, reducing h also increases the prevalence of shear cracking in the vicinity of the 45° point on the hole boundary. This suggests that activation of the shear failure mechanism also becomes more likely as h decreases.

Also of note in the plot of matrix cracking is the extent of matrix cracking in the shorter strut at its failure load: unlike the longer strut, the shorter strut fails before the region over which matrix cracking occurs spreads across its entire width. The resulting reduction in energy absorption is reflected in the failure loads. The analyses indicate that a strut with $h/r = 4$ fails at a remote stress $P/(2w)$ of $1.14\sigma^0_{mc}$, where P is the force per unit thickness. The failure load predicted for the strut with $h/r = 2$, which fails while matrix cracking is still fairly localized, is just over half of this at $P/(2w) = 0.64\sigma^0_{mc}$.

3.2.2 STRUT WIDTH, w/r

To assess the effect of strut width on the way SiC/MAS struts carry loads, a strut is analyzed with $h/r = 2$, as above, but with $w/r = 10$. Again, the bolt is taken to be rigid, and the interface is frictionless. Considering the material between the top of the bolt and the upper edge of the strut as a beam on a deformable foundation, the expectation is that increasing the width of the strut will increase the stiffness of the "foundation," and thus mitigate the stress concentration at the top of the wider strut. As illustrated by Figure 7, this is indeed the case. With the reduction in the stress concentration at the top of the strut, the failure mechanism predicted by the maximum normal strain criterion for the wide strut shifts to tensile failure at the hole boundary. However, the plot of matrix cracking for this strut shows that cracking is actually most intense in shear, near the 45° point on the hole boundary; the shear failure mechanism might be close to activation in this case.

While the narrower strut withstands a higher average stress $P/2w$ at failure than does the wider strut, the analysis predicts that the force per unit depth of $P/h = 2.7\sigma^0_{mc}$ necessary to break the wider strut just exceeds the failure strength $P/h = 2.6\sigma^0_{mc}$ of the narrower strut.

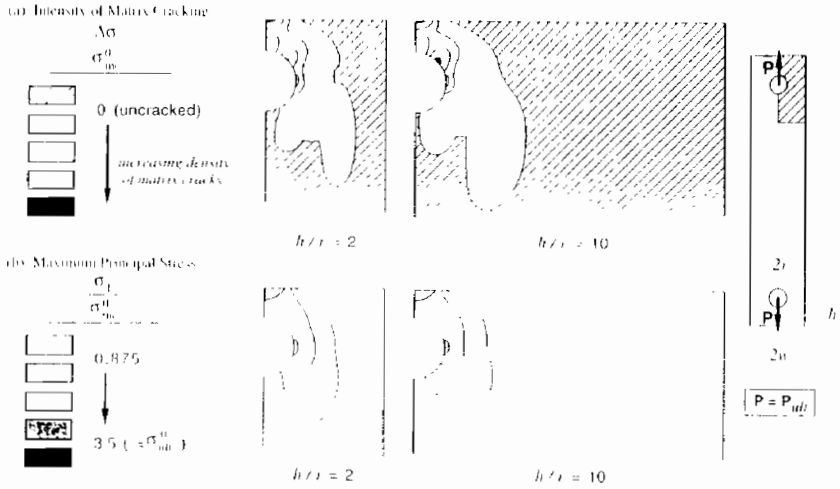

Figure 7. *Effect of strut width w on (a) matrix cracking and (b) stress distribution at failure load,* P_{ult}; h/r = 2.

3.2.3 DISCUSSION

The predicted failure mechanism of a strut changes with the strut's relative dimensions. The trends found in this section are qualitatively similar to those observed experimentally by Cady et al. [12]. The observations of Cady et al., that the shear mode of failure becomes increasingly dominant with increasing specimen width and that the normal mode of failure becomes increasingly dominant with increasing specimen length were both replicated in these analyses. The bending mode of failure is predominant when the bolt is placed near the upper edge of the strut and when the strut is too narrow for its width to contribute significantly to the bending stiffness of the material above the bolt. None of the experimental work on CMCs cited in this paper reported observing bending failure, but the strut for which this failure mode was predicted here was beyond the range of specimen sizes considered in any of these investigations.

3.3 Interfacial Friction

The role of interfacial friction is assessed by analyzing a strut with dimensions $h/r = 4$ and $w/r = 4$ identical to that analyzed in Section 3.2.1, but with the condition imposed that nodes which are in contact with the rigid bolt remain fixed. This provides an upper bound on the frictional force along the interface between the bolt and the strut.

Interfacial friction constrains material directly above the bolt from stretching horizontally (i.e., perpendicular to the direction of loading), and thereby greatly reduces stresses above the bolt, as is shown in Figure 8. However, the reduction in

stresses above the bolt means a reduction in stress redistribution by matrix cracking, and results in an overall decrease in the load-carrying capacity of this strut. Friction intensifies the stress concentration at the hole boundary, and reduces the failure load by about 50%.

For this strut, a no-slip boundary condition along the interface completely suppresses the bending mode of failure, and also reduces the level of shear cracking, as can be seen from Figure 8. The strut will fail in the tensile mode, with a high degree of certainty.

3.4 Bolt Elasticity

A strut with dimensions $h/r = 4$ and $w/r = 4$ is again loaded, this time with soft, frictionless bolts having an elastic modulus one tenth that of the strut. The region of contact between bolt and strut is broadened by allowing the bolt to deform, and this causes a slight reduction in stresses above the hole. The failure mechanism is unaffected by the elasticity of the bolt. This result concurs with that of Hyer et al. [3], for linear elastic struts.

The elasticity of the bolt plays a larger role when interfacial friction is incorporated into the problem. Two identically dimensioned struts, both with no slippage allowed for surfaces in contact, are pictured at their failure loads in Figure 9. One strut is loaded by a rigid bolt, while the other is loaded by a soft bolt, with

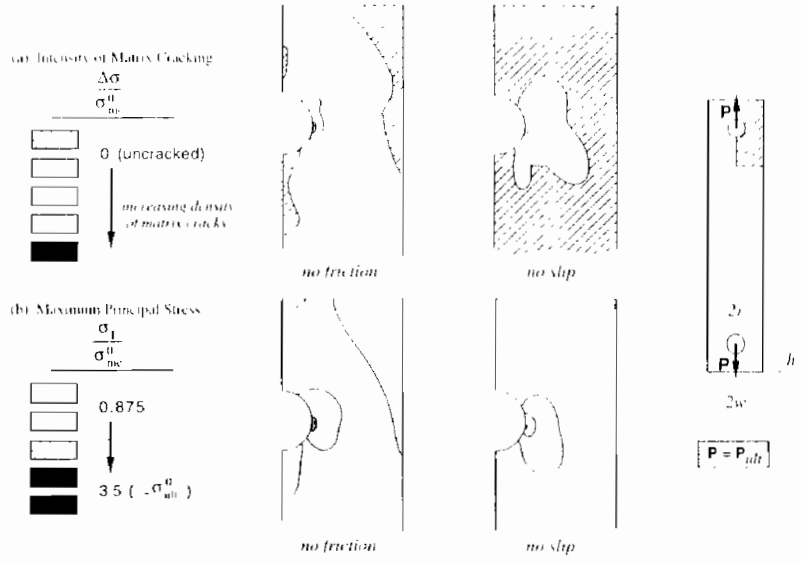

Figure 8. *Effect of interfacial friction on (a) matrix cracking and (b) stress distribution at failure load,* P_{ult}; h/r = 4, w/r = 4.

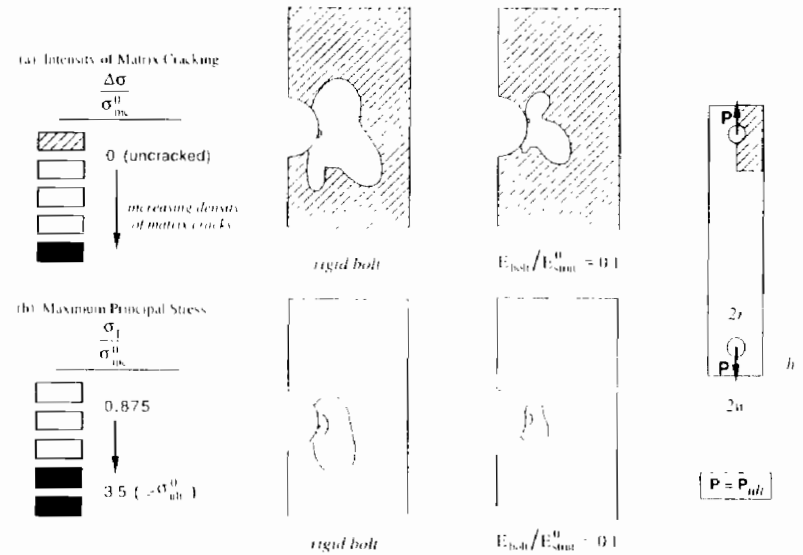

Figure 9. *Effect of bolt elasticity on (a) matrix cracking and (b) stress distribution at failure load, P_{ult}; when no slippage is allowed between the bolt and the strut* h/r = 4; w/r = 4.

$E_{bolt}/E_{strut} = 0.1$. As can be inferred from Figure 9, the soft bolt moves the end of the region of contact and the point of maximum stress closer to the thinnest section of the strut, and thereby reaises the stress concentration. The bolt elasticity results in over a 10% drop in the failure load of the strut. This is likely to be a larger effect than would be seen in a real strut, as the model of friction applied here is idealized.

3.5 Discussion

Bolt-loaded struts analyzed in this section are predicted to fail through the "shear," "tensile," and "bending" modes illustrated in Figure 3. The "shear" and "tensile" modes match qualitative experimental observations reported by Cady et al. [12], but the "bending" mode has no observational support. The bending failure has most likely eluded experimental observation partially through interfacial friction, which completely precludes this failure mechanism for the extreme case evaluated here, and partially through the common sense of those who have sought to characterize these failure mechanisms experimentally: achieving this failure mechanism requires drilling a hole far closer to the top of a strut than any engineer would realistically consider.

Comparisons of the predicted failure mechanisms to the locations of intense matrix cracking indicates that the failure criterion used in this section either over-

predicts the shear strength of the SiC/MAS composite, or underpredicts its tensile strength. The former is likely. Regardless of which is the case, the design engineer forced to utilize this failure criterion would now seek to design a strut that avoids the nonconservatively predicted "shear" mode, and optimizes this design based on the specific material properties of the SiC/MAS laminate.

Interfacial friction should be avoided to the extent possible when designing attachments for the SiC/MAS cross-ply. If friction is minimized, the elasticity of the bolt has no significant bearing on design.

4. DESIGN OPTIMIZATION BASED UPON MATERIAL PROPERTIES

Rather than continue with the bolted strut analyzed in Section 3, attention is turned to the more interesting, but mathematically similar problem of a bolted plate illustrated in Figure 2. A plate is loaded by bolts in the direction shown. The infinitely-wide plate is long compared to the bolt spacing $2s$, and is symmetric about a horizontal line through its center. The bolts are allowed to slide freely in the lateral direction, and are each pulled vertically with a force $(2s)\sigma$. The goal here is to find the bolt spacing s that best utilizes the nonlinearity of the SiC/MAS composite to maximize the plate's strength. Based on the analysis of the strut in Section 3, a depth $h/r = 4$ is used, as this was a bolt depth for the strut at which a tensile failure in the strut was very probable. Once an optimal spacing is ascertained, the failure mechanism corresponding to this spacing is carefully checked.

4.1 Numerical Procedure

The boundary value problems are once more solved using the finite element method in conjunction with the constitutive model presented in Section 2. The model is again fit to McNulty and Zok's material data for the SiC/MAS cross-ply.

For each bolt spacing s considered, a finite element mesh is generated according to the model in Figure 2(b). This model is identical to that used for the strut, except here the nodes on the right-hand boundary are constrained to move together in the horizontal direction. This models both the periodicity of the problem, and the condition that the bolts may move laterally.

The bolts are taken to be rigid, and the interface carries no friction. As before, the boundary conditions are part of the solution, and iteration is required even for loads to which the plate responds linearly.

4.2 Results

Failure loads for plates with a range of bolt spacings are calculated, and are plotted in Figure 10, normalized by the highest failure load that can be achieved by a

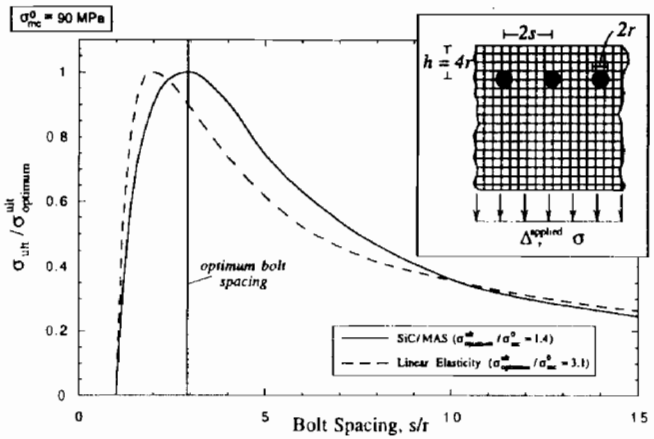

Figure 10. *Ultimate load of a fastened SiC/MAS plate as a function of bolt spacing s/r, compared to the ultimate loads for a linear plate having the elastic properties of SiC/MAS; h/r = 4.*

bolted SiC/MAS plate. This peak load of $\sigma = 1.4\,\sigma^0_{mc}$ occurs when the bolt spacing $2s$ is approximately six times the bolt radius.

To highlight how stress redistribution related to matrix cracking influences the optimum dimensions of a bolted plate, a similar analysis is run with the plate taken as linear elastic. The failure loads for a linear elastic plate having the elastic constants of SiC/MAS are plotted with a dashed line in Figure 10, normalized by the highest possible failure load that can be attained with such a plate. For a brittle plate with same failure strain as the SiC/MAS composite, this peak load is $\sigma = 3.1\sigma^0_{mc}$. The optimum bolt spacing 2s for the linear elastic plate is four times the bolt radius: the strongest SiC/MAS plate is constructed with two times as much material between edges of neighboring bolts as the strongest elastic plate.

The optimum bolt spacing for the SiC/MAS plate is reached by the following trade-off. As the bolt spacing decreases, the cross-sectional area between neighboring bolts decreases. However, the average stress across this area increases as the bolt spacing decreases for two reasons: first, the elastic stress concentration drops (relative to the mean stress across the ligament), and second, the redistribution of stresses away from these concentrations due to the mechanism of matrix cracking increases. This is illustrated in Figure 11, which shows the increase in the average stress between neighboring bolts for decreasing bolt spacing. As s approaches the bolt radius, the net section stress at failure approaches the uniaxial failure stress of $3.5\sigma^0_{mc}$.

Analysis of an SiC/MAS plate with a nearly optimal bolt spacing indicates that

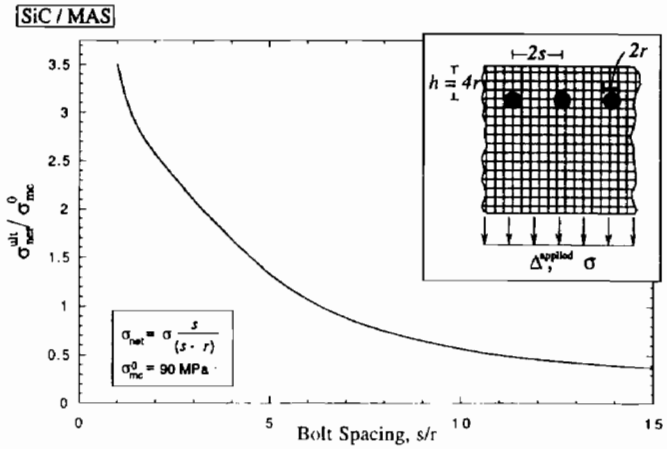

Figure 11. *Performance of a fastened SiC/MAS plate as a funciton of bolt spacing s/r; h/r = 4.*

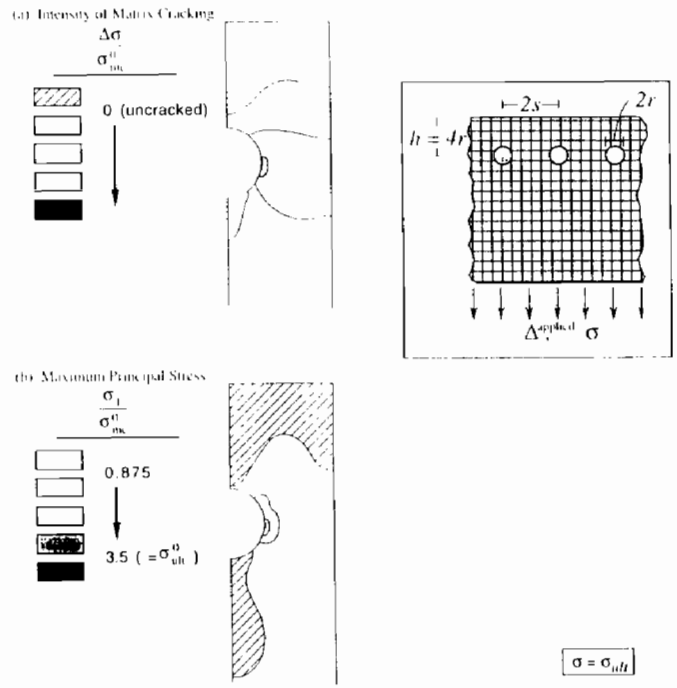

Figure 12. *(a) Intensity of matrix cracking and (b) stress distribution at failure, σ_{ult}, for optimal bolt spacing s/r = 3; h/r = 4.*

at the optimum dimensions, the plate fails in the "tensile" failure mode. As can be seen from Figure 12, which displays contours of principal stresses and matrix cracking at the failure load for material in close proximity to the bolts, the increase in the bending stiffness of material above the bolts caused by the periodic boundary conditions eliminates any chance of a "bending" failure. Since shear cracking is also not prevalent, the tensile failure mechanism is likely to be the only possible failure mechanism for this configuration.

5. SUMMARY

Assuming a simple failure criterion, this work explored the effect of geometric and material parameters on failure loads and mechanisms of a bolted CMC strut undergoing matrix cracking. As the position of a bolt in a fairly wide strut nears the end of the strut, the likely failure mode shifts from a tensile mode to a shear mode. For more narrow struts, a "bending" mode can occur. Friction along the bolt-strut interface promotes the tensile failure mode, and also significantly reduces a strut's load-carrying capacity. The elastic properties of the bolt have little bearing on load-carrying capacity, especially if friction is minimized.

The analysis technique used herein can be used to optimize design of fasteners. In the case examined here, the optimal design of a uniformly fastened CMC plate is reached through a trade-off between decreasing area between neighboring bolts, and increasing stress redistribution due to matrix cracking.

ACKNOWLEDGEMENTS

The authors would like to thank Carl Cady and Tony Evans for helpful discussions of their experimental observations [12], and John McNulty and Frank Zok for furnishing data for the model CMC used in this study.

This work was supported in part by the ARPA University Research Initiative (Sub-agreement P.O. KK-3007 with the University of California, Santa Barbara, ONR Prime Contract N00014-92-J1808) and the Division of Applied Sciences, Harvard University.

REFERENCES

1. G. M. Genin and J. W. Hutchinson. "Composite Laminates in Plane Stress: Constitutive Modeling and Stress Redistribution due to Matrix Cracking," *J. Am. Ceram. Soc.*, 80(5):1245–1255 (1997).
2. J. P. Waszczack and T. A. Cruse. "Failure Mode and Strength Prediction of Anisotropic Bolt Bearing Specimens," *J. Compos. Mater.*, 5:421–423 (1971).
3. M. W. Hyer, E. C. Klang, and D. E. Cooper. "The Effects of Pin Elasticity, Clearance, and Friction on the Stresses in a Pin-Loaded Orthotropic Plate," *J. Compos. Mater.*, 21:190–206 (1987).
4. F.-K. Chang, R. A. Scott, and G. Springer. "Failure Strength of Composite Laminates Containing Pin-Loaded Holes—Method of Solution," *J. Compos. Mater.*, 18:255–278 (1984).

5. W. Bickley. "The Distribution of Stress Round a Circular Hole in a Plate," *Phil. Trans. Roy. Soc. A*, 227:383 (1928).
6. T. De Jong. "Stresses Around Pin-Loaded Holes in Elastically Orthotropic or Isotropic Plates," *J. Compos. Mater.*, 11:313–331 (1977).
7. B. L. Agarwal. "Static Strength Prediction of Bolted Joint in Composite Material," *AIAA Journal*, 18:1345–1375 (1980).
8. R. E. Rowlands, M. U. Rahman, T. L. Wilkinson, and Y. I. Chang. "Single- and Multiple-Bolted Joints in Orthotropic Materials," *Composites*, 13:273–278 (1982).
9. K.-D. Zhang and C. E. S. Ueng. "Stresses Around a Pin-Loaded Hole in Orthotropic Plates," *J. Compos. Materials*, 18:432–446 (1984).
10. S. M. Serabian and D. W. Oplinger. "An Experimental and Finite Element Investigation into the Mechanical Response of 0/90 Pin-Loaded Laminates," *J. Compos. Mater.*, 21:631–649 (1987).
11. F.-K. Chang, R. A. Scott, and G. S. Springer. "Failure Strength of Nonlinearly Elastic Composite Laminates Containing a Pin Loaded Hole," *J. Compos. Mater.*, 18:464–477 (1984).
12. C. M. Cady, A. G. Evans, and K. E. Perry. "Stress Redistribution Around Mechanical Attachments in Ceramic Matrix Composites," to appear in *J. Am. Ceramic Soc.*
13. M. Y. Tsai and J. Morton. "Stress and Failure Analysis of a Pin-Loaded Composite Plate: An Experimental Study," *J. Compos. Mater.*, 24:1101–1120 (1984).
14. F. L. Matthews, A. A. Roshan, and L. N. Phillips. "The Bolt Bearing Strength of Glass/Carbon Hybrid Composites," *Composites*, 13:225–227 (1982).
15. J. C. NcNulty and F. W. Zok. "Application of Weakest-Link Fracture Statistics to Fiber-Reinforced Ceramic Matrix Composites," to appear in *J. Am. Ceramic Soc.* (1997).
16. J. C. McNulty and F. W. Zok. Private communication.
17. G. M. Genin, J. W. Hutchinson, J. C. McNulty, and F. W. Zok. "Shear Characterization of Brittle Matrix Cross-Ply Laminates Using the Iosipescu Shear Test," in preparation.
18. N. A. Fleck. "Compressive Failure of Fiber Composites," *Advances in Applied Mechanics*, New York: Academic Press, 33:43–119 (1997).
19. B. Budiansky. "On the Theoretical Toughness and Strength of Ceramic Composites," Proceedings of IUTAM Symposium on Fracture of Brittle Disordered Materials: Concrete, Rock, Ceramics, Brisbane, September 20–24 (1993).
20. B. Budiansky and J. C. Amazigo. "Notch Strength of Ceramic Composites: Long Fibers, Stochastics, Short Fibers," Harvard University Solid Mechanics Report MECH-269.
21. D. Beyerle, S. M. Spearing, and A. G. Evans, "Damage Mechanisms and the Mechanical Properties of a Laminated 0/90 Ceramic Matrix Composite," *J. Am. Ceram. Soc.*, 75:3321–3330 (1992).
22. B. Harris, F. A. Habib, and R. G. Cooke, "Matrix Cracking and the Mechanical Behaviour of SiC-CAS Composites," Proc. R. Soc. Lond., 437:109–131 (1992).